Short article

Structure

The mechanosensitive channel YbiO has a conductance equivalent to the largest gated pore

Graphical abstract

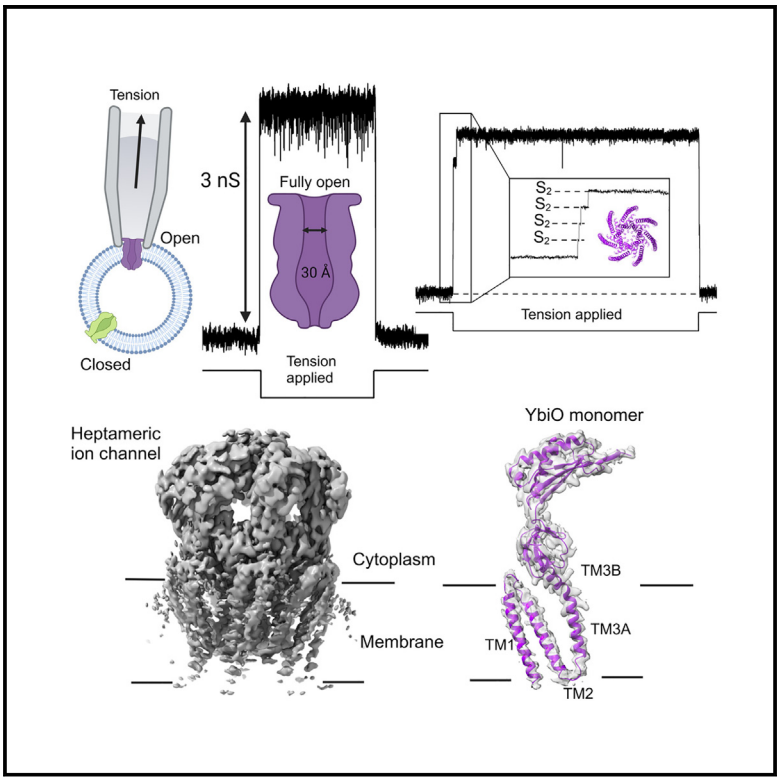

Authors

Benjamin J. Lane, Mariangela Dionysopoulou, Nana Yan, Jonathan D. Lippiat, Stephen P. Muench, Christos Pliotas

Correspondence

christos.pliotas@manchester.ac.uk

In brief

Lane et al. demonstrate that the mechanosensitive channel YbiO can achieve conductances equivalent to the largest gated-pore in nature when subjected to membrane tension. Single-channel analysis shows that YbiO has multiple biologically relevant substates. The pore dimensions of our YbiO structure are consistent with a substate identified in electrophysiology recordings.

Highlights

- YbiO can achieve a conductance of ~3 nS equivalent to the largest gated-pore MscL
- Electrophysiological characterization of YbiO shows multiple conducting states
- A structure of YbiO representing a subconducting state was determined by cryo-EM

Lane et al., 2025, Structure *33*, 652–662
April 3, 2025
https://doi.org/10.1016/j.str.2025.01.014

CellPress

CellPress
OPEN ACCESS

Structure

Short article

The mechanosensitive channel YbiO has a conductance equivalent to the largest gated pore

Benjamin J. Lane,[1,2,3] Mariangela Dionysopoulou,[1,2] Nana Yan,[1,2] Jonathan D. Lippiat,[2] Stephen P. Muench,[1,2] and Christos Pliotas[1,2,4,5,6,*]

[1]Astbury Centre for Structural Molecular Biology, University of Leeds, Leeds LS2 9JT, UK
[2]School of Biomedical Sciences, Faculty of Biological Sciences, University of Leeds, Leeds LS2 9JT, UK
[3]Aston Institute for Membrane Excellence, Aston University, Birmingham B4 7ET, UK
[4]School of Biological Sciences, Faculty of Biology, Medicine and Health, The University of Manchester, Manchester M13 9PT, UK
[5]Manchester Institute of Biotechnology, The University of Manchester, Manchester M1 7DN, UK
[6]Lead contact
*Correspondence: christos.pliotas@manchester.ac.uk
https://doi.org/10.1016/j.str.2025.01.014

SUMMARY

Bacterial mechanosensitive channels are divided into large (MscL) and small (MscS-like) conductance families. The function of MscS and MscL is to protect cells against osmotic shock by acting as pressure safety valves. Within the MscS-like family, *E. coli* encodes much larger channels, such as YbiO, MscK, and MscM, but their physiological role remains unclear. Compared to MscL their conductances are reported as 3–10 times lower. We show that YbiO can achieve a conductance of ~3 nS, and an equivalent pore opening of > 25 Å in diameter, equaling the known largest gated pore, MscL. We determine a cryoelectron microscopy (cryo-EM) structure of YbiO in a sub-open conformation, demonstrating the existence of multiple substates. One substate is consistent with the pore opening extent of our structure and the other matches states previously thought to resemble full openings. Our findings demonstrate surprising capabilities, hinting at new physiological roles for YbiO and potentially other MscS-like channels.

INTRODUCTION

Membrane proteins have evolved alongside lipid molecules, and consequently, their structure and function are altered by the chemical and physical properties of the bilayer. For mechanosensitive (MS) channels this lipid-protein relationship is even more intimate, as these systems sense and respond to tension changes in the bilayer, and direct interactions with the membrane have been shown to be key in their gating mechanisms.[1–5] In bacteria, seven MS channels (MscL, MscS, YnaI, YbdG, MscK, MscM, and YbiO) have been identified.[6–9] These channels can be grouped into two major families, MscL and the rest under the umbrella of the MscS-like family. Bacterial MS channels sense changes in lateral tension generated in the membrane during hyperosmotic shock, allowing bacteria to release solutes to prevent cell lysis.[10–13] However, their redundancy implies that some of these channels may serve other fundamental roles in bacterial physiology,[10,14] and several of them are known to be implicated in bacterial pathogenicity and possess additional functionalities.[15–20] For example, MscK is potassium dependent, and YbiO, MscK, and MscM all have an additional periplasmic domain and an extended transmembrane (TM) domain, the functional role of which is unknown.[7,8] Several models have been suggested for the sensing of membrane forces by an ion channel.[2] The most substantiated model in bacterial and several eukaryotic channels is the lipid-moves-first model,[4,5] which provides a molecular basis for the more general force-from-lipid principle.[21] This entropy-driven model proposes that there are membrane tension-sensitive domains in MS channel proteins, which in the case of MscL and MscS, exist as TM pockets which are directly implicated in their mechanical sensing and response.[4,22,23] Notably, similar TM lipid pockets also exist in larger MscS-like channels and are key to their gating.[24–28]

Studies to address aspects of the YbiO channel structure and function are extremely limited. As a member of the MscS-like superfamily, YbiO is heptameric and this was evidenced in a partial structure of its MscS-like domain.[7,24] YbiO is predicted to have 11 TM helices per subunit. The MscS-like TM1 and TM2 are expected to form a flexible sensing paddle, with TM3 as the pore lining helix and lipid pockets in between. The periplasmic domain of YbiO has no sequence similarity outside of closely related species.[7] Initial electrophysiological studies of YbiO have been performed in protoplasts, reporting conductances in the range of 16–19 pA (0.8–1.0 nS) with a pressure ratio (PMscL:PYbiO) of ~1.16–1.21 required for gating.[7,24] YbiO is induced by NaCl, and its expression is dependent on RpoS.[7] RpoS is a sigma

factor which are a group of proteins that regulate transcription in bacteria in response to different environmental stimuli. RpoS controls the synthesis of many stationary phases and osmotically induced genes and is a key regulator of the general stress response in bacteria.[7,29–31] The complex regulation of YbiO is not fully understood, but it is not incorporated into the membrane at sufficiently high levels to afford protection from osmotic shock under physiological conditions, which leaves open questions about its primary function. Limited studies have suggested that it potentially has a role in influencing the pathogenicity of bacteria.[17,18] In one of these studies, *Salmonella* strains associated with epidemic outbreaks were found to have 7 gene variants compared to non-epidemic-causing strains, including a Gly602Arg single-nucleotide mutation in YbiO.[17] Therefore, further investigations into YbiO may identify it as a potential target for antimicrobial resistance.

Of the largest *E. coli* MscS-like channels (11 TM helices per subunit) only MscK has been structurally characterized in both a closed and open state.[26] MscK is unique due to the requirement of external ions (K^+, Rb^+, or Cs^+) in addition to lateral tension for gating.[8,32,33] MscK is the largest known bacterial MS channel and has a significantly larger (~500 residues) periplasmic domain than YbiO, and like YbiO, has 11 TM helices per subunit (e.g., 77 TM helices per channel).[26,34–36] The structures show that MscK comprises three layers: a C-terminal cytoplasmic domain, a curved TM domain, and an N-terminal periplasmic ring.[26] As has been seen for YnaI, YbiO, and MSL1, the cytoplasmic domain is structurally conserved.[24,25,37,38] The periplasmic domain of YbiO is unlikely to form the helical bundles seen in MscK, as it has a significantly smaller number of residues, lacks sequence similarity outside closely related species,[7] and AlphaFold[39] analysis gives low confidence scores for the modeling of this region (Figure S9). In MscK, there is a curvature in the arrangement of the TM helices, reminiscent of that seen in Piezo channels.[26] Several plant MscS-like channels, such as MSL1, MSL10, and FLYC1 have been structurally characterized,[25,27,37,40–42] and their extended TM domains also feature variable degrees of membrane curvature, with MSL1 particularly presenting high TM curvature in the closed state, which flattens upon opening, suggesting a role in sensing and responding to curvature changes in membranes.[37]

Here, we report single-channel conductances of the YbiO channel in giant unilamellar vesicles (GUVs), equivalent to that of MscL, currently the largest known gated pore in nature. Our findings create a precedent for other MscS-like channels to be revisited to identify their unique biophysical properties and roles. We also report additional single-channel activities of lower conductances, which resemble biologically relevant substates of YbiO, previously assigned as full channel openings. Finally, we determine a cryoelectron microscopy (cryo-EM) structure of the heptameric YbiO channel, consistent with one of these intermediate sub-open states (PDB: 9GO3, EMDB:51489).

RESULTS

Single-channel YbiO recordings show equivalent conductances to MscL-like openings

Limited electrophysiological studies of YbiO have been done in protoplasts which reported conductance in the range of 16–19 pA (0.8–1.0 nS) with a pressure ratio (PMscL:PYbiO) of ~1.16–1.21 required for gating.[7,26] Studies of MscK and MscM in spheroplasts have also shown conductances of ~0.9 nS and ~0.3 nS respectively.[7,8,26] We purified recombinantly expressed wild-type (WT) YbiO and reconstituted the protein into Soy-PC giant unilamellar vesicles (GUVs) for functional characterization by single channel electrophysiology. We selected the GUV set-up because, despite being technically challenging, it allows the study of pure and monodisperse YbiO in the absence of other cellular and membrane components. We also used Soy-PC, which is an established lipid system for the study of bacterial MS ion channels.[22,43–47] Prior to YbiO recordings, we first performed control measurements under applied tension of empty GUVs and GUVs loaded with WT MscS (Figure S1). No activities were detected following the application of negative pressure in empty GUVs (Figure S1A). Control patch-clamp electrophysiology measurements of WT MscS channels in GUVs of the same lipid composition were consistent with biologically relevant MscS activities previously reported in a variety of systems (e.g., spheroplasts, protoplasts, and GUVs) (Figure S1B).[9,43,47,48] We then reconstituted WT YbiO into Soy-PC GUVs for electrophysiological characterization under applied tension. While we initially observed comparable conductances to those previously reported in protoplasts for YbiO in our GUVs set up,[7,24] and here defined as "S_2", we also observed an additional range of significantly larger single channel conductances consistent with the presence of multiple intermediate states, as previously shown for both MscS and MscL.[23,46,49–51] These larger conductances are defined as subconducting state S_1 and fully open (FO). Conductances of 0.57 nS (±0.10) (S_2) (n = 4), 2.09 nS (±0.40) (S_1) (n = 4), and 2.97 nS (±0.36) (FO) (n = 5) were measured for WT YbiO (Figures 1 and S7). The pressure activation threshold required for full channel opening was 90 ± 34.1 mmHg. Interestingly, all the full openings we observed from independent GUV patches (n = 5, YbiO) were acquired at substantially higher pressure thresholds than the ones required for MscS and other MscS-like channels. This is consistent with electrophysiology studies on YbiO in spheroplasts that required near MscL pressure thresholds to reach its reported ~1 nS conductance.[7] Conductances for S_2 and S_1 were 0.57 nS (±0.10) (n = 4) and 2.09 nS (±0.40) (n = 4) with pressure thresholds of 92.5 mmHg (±31.1) and 70 mmHg (±30), respectively (Figures 1 and S7). A summary of these values can be found in the supplemental (Table S2).

Structural characterization of YbiO in a sub-open state using cryo-EM

To explore YbiO's structural architecture and the conformational rearrangements that were occurring to give rise to a wide range of ion conductances, we employed cryo-EM and determined the structure of YbiO (Table 1). In our solved structure the channel adopts a previously unseen state, as judged by the pore diameter at the constriction site and shifts in TM helices (Figure 2D). The previously reported structure of YbiO (7A46) only had part of TM1 and TM2 modeled, without the connecting loops.[24] Therefore, our structure is the most complete to date as it has allowed for the determination of multiple previously unresolved TM residues. In the cryo-EM micrographs and the 2D classes (Figure 2F), consistent with other structures of MscS-like channels, a cone-like shape of the extended TM domain is visible, but

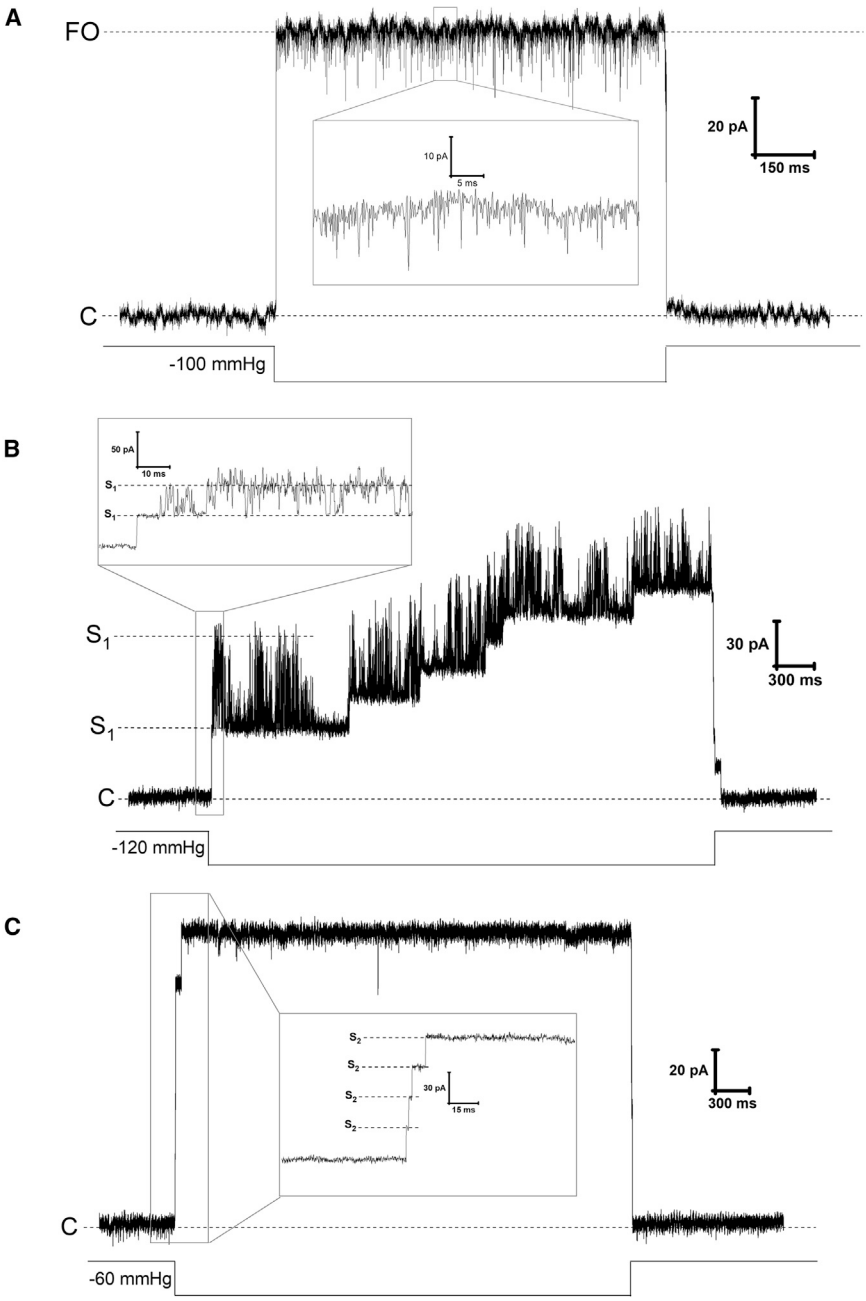

Figure 1. Representative patch-clamp recordings of YbiO reconstituted into Soy-PC GUVs, recorded at +30 mV membrane potential

"*n*" is the number of individual patches.

(A) Representative recording of the fully open state of YbiO measured in GUVs. This state has a mean conductance of 2.97 nS (±0.36) (*n* = 5) where "*n*" is the number of individual patches. The scale bar corresponds to 20 pA and 150 ms. Figure 1A is related to Figure S2 as both measurements are from the same patch. Figure 1A represents the first stable opening at 100 mmHg. Figure S2 shows the initial activity observed at 80 mmHg, but the channel did not achieve a stable opening for the entire duration of tension application, requiring higher pressure for this.

(B) Representative recording for the subconducting S_1 state measured in GUVs. This state has a mean conductance of 2.09 nS (±0.40) (*n* = 4). The scale bar corresponds to 30 pA and 300 ms.

(C) Represents recordings of the subconducting S_2 state of YbiO, with several channels transitioning into this S_2 state following the application of pressure. This state is close to one previously reported for YbiO in spheroplasts[7] and has a mean conductance of 0.57 nS (±0.10) (*n* = 4). The scale bar corresponds to 20 pA and 300 ms.

high-resolution information is lacking, likely because of the high flexibility of the outer TM helices. A similar lack of density for the outer helices has previously been reported in a cryo-EM structure of the smaller of MscS-like channel YnaI.[54] 2D classes of YbiO where the TM domain is at different angles (Figure 2F) suggest YbiO could respond to membrane curvature changes. From our cryo-EM map, a model of the MscS-like core, including the entire cytoplasmic domain and multiple TM segments could be built. In the TM domain, we were able to model TM3A and B, TM2, and most of TM1 with the connecting loops between these helices and newly register a large number of the residues within the helices (Figure 3). The TM domain contains the pore-lining helix TM3B which controls the channel gate and the extent of pore opening and could be linked to distinct functional states (Figure S3). Structural alignment of our YbiO structure with the previously reported structure (PDB: 7A46), and comparison of HOLE pore diameter analysis, suggest our structure is in a different state (Figures 2D and 2E).[24,55]

Flegler et al. (2020) reported a partial structure of YbiO in a closed-like state. However, Channel Annotation Package (CHAP) and molecular dynamic (MD) simulation analysis suggested the pore was hydrated and ion-conducting.[24,56] Comparison of the YbiO model with closed MscS (PDB: 6VYK), showed that the overall core structure is conserved with a cytoplasmic vestibule domain, pore-forming TM3 helix, and the paddle formed by TM1 and TM2 (RMSD = 3.043) (Figure S8).[24,49] This is also in agreement with the published structure of YnaI and MscK.[24,26] Compared to closed MscS, TM1 and TM2 are similar but rotated by ∼20°–25° and are tilted slightly away from the central axis of the pore (Figure S8). It was previously predicted that YbiO has a 19-residue loop between TM1 and TM2 in comparison to a 6-residue loop in MscS.[24] However, our structural data are inconsistent with this prediction, as the TM1-TM2 loop is half the size in our current YbiO model, with the rest forming part of ordered TM helices. Interestingly, there is extra non-protein density in the coulomb potential map which sits between TM1 and TM2 from one chain (e.g., A) and TM2 of the neighboring chain (e.g., B) (Figure 2C). While the overall resolution of

Table 1. Cryo-EM data collection parameters

	WT YbiO GDN/CHS
Detergent concentration (%)	GDN/CHS 0.042/0.0042
Detector	Falcon 4i
Energy filter (eV)	10
Voltage (kV)	300
Defous range (μm)	−1.0, −1.2, −1.4, −1.6, −1.8, −2.0
Magnification (×)	165000
Pixel size (Å)	0.74
Dose per physical pixel/second ($e^- s^{-1}$) per second	6.02/6.37/6.59[a]
Total dose (e/Å^2)	66/70.8/65.8[a]
Initial particle images	1.7 million
Final particle images	147K
Resolution (Å)	3.15

[a]Multiple individual data collections from the same grid were combined following particle extraction.

the map is 3.15 Å (Figure S5B), the resolution drops to 4–4.5 Å in this region and therefore we could not unambiguously assign this density (Figures 2C and S5C). However, the location of this additional non-protein density within the TM domain between helices TM2 and TM3 is consistent with lipid density also found in many other MscS-like and MscL channels, where lipids present in pockets formed between TM helices play a key role in mechanical sensing and response.[1,2,4,5,22–24,26,28,37,38,57]

Both the constricting residues that are the final stopping point for hydration and conduction of the ion channel could be visualized—L549 and F553 (Figures 3C and 3D). These residues are close to the cytoplasmic domain of the protein and at the interface of the inner-membrane plane, and their side chains point into the pore axis and form the narrowest points. Pore analysis using HOLE[55] shows that our structure has a pore diameter of ∼9.5 Å at the narrowest point F553. Such a diameter could allow for water molecules to pass through, therefore suggesting our structure is not fully closed. HOLE analysis of the closed-like structure (PDB: 7A46) revealed a smaller diameter at the pore constriction site (∼6.7 Å), compared to our structure (PDB: 9GO3); however, computational electrophysiology experiments within their study suggested the closed-like channel was able to conduct ions, and this was accompanied by slight rotation of the TM helices, consistent with the state not being completely closed.[24] Our structure presents an increase in pore diameter of ∼2.8 Å compared to the previous closed-like structure and is consistent with a sub-open state.[24] Structures resembling closed states of MscS, such as PDB: 2OAU and PDB: 6VYK, have pore diameters of ∼4.95 Å and ∼5.34 Å, respectively, at the tightest constricting residue (L105).[49,58] Our YbiO structure has a substantially increased pore diameter compared to both closed MscS states and the previously reported YbiO closed-like state (PDB: 7A46), which had rotation in the TM helices, consistent with it not being fully closed. On this basis, our YbiO structure (PDB: 9GO3) most likely resembles an intermediate state and is more consistent with the electrophysiological S_2 state. According to the ∼3 nS single channel conductance we recorded here, a YbiO FO state is estimated to have a pore diameter of >25 Å, based on previous calculations for MscL.[45,51,59]

A single G602R mutation in YbiO has been associated with increased pathogenicity of bacteria.[17] At a resolution of ∼2.8 Å, we can visualize this region in our structure and conclude that this mutation site sits on a loop across the cytoplasmic portals and remains unchanged between the closed-like (PDB: 7A46) and sub-open (PDB: 9GO3) YbiO structures (Figures 3B and 3F), with little movement occurring within the cytoplasmic domains between the two states.[24] This suggests that this region is probably unaffected by channel gating and any functional effects associated with this site may be due to the charges and/or additional bulkiness this particular mutation introduces.

DISCUSSION

Seven MS channels have been identified in *E. coli*, and the smaller channel proteins MscL and MscS provide the majority of protection against osmotic shock. So far, the rest of the larger *E. coli* MscS-like channel proteins seem to have a redundant role in this function.[7,8,14] Structural and functional studies of the larger members are very limited.[60–62] Recently, the structure of the larger *E. coli* MscS-like channel MscK was determined.[26] This channel showed changes in the curvature of its TM domain between two states, forming a dome-like structure which is reminiscent of that seen for the eukaryotic Piezo channels.[63–66] YbiO is predicted to have the same number of TM helices as MscK and likely a dome-like indentation in the TM domain. Our 2D classes for YbiO show substantial changes in the curvature of the TM domain (Figure 2F). This structural architecture is also consistent with other eukaryotic MscS-like channels that possess extended TM domains found in plants and fungi.[25,27,36,37,57] Curvature dependence may be a key characteristic among the larger members of the MscS-like superfamily. According to the entropy-driven lipid-moves-first model,[2,4,5,67] lipid movement from TM pockets formed by their TM3/TM2, is expected to play a central role in the mechanisms of these larger channels, however, it may also be that membrane curvature has a synergistic effect in channel gating.[24,26,28,68]

To date, the smallest size MS channel in bacteria, MscL, is known to form the largest gated pore in nature. MscL is predicted to have an open pore diameter of 28–40 Å with a measured conductance of ∼3 nS, allowing the passing of small (∼10 kDa) proteins through its non-selective pore,[59,69] making it an ideal system for biotechnological exploitations.[70] As of now, these pore openings were thought to be unique with no other single-channel gated pore having the structural capability to reach these ion conductance values. YbiO is one of the largest members of the MscS family, but data for its role in bacterial physiology is scarce. Previously, YbiO's activity was examined in protoplasts and maximum openings of ∼1 nS were recorded, like those of MscS, but a higher-pressure activation threshold was required.[7] The conductance of the channel has never been tested on monodisperse purified channel proteins reconstituted in giant unilamellar vesicles (GUVs), devoid of other membrane proteins. Surprisingly, in our electrophysiology GUV experiments we observed that at high (close to lytic) tension, YbiO presents very large openings, equal to that of the single

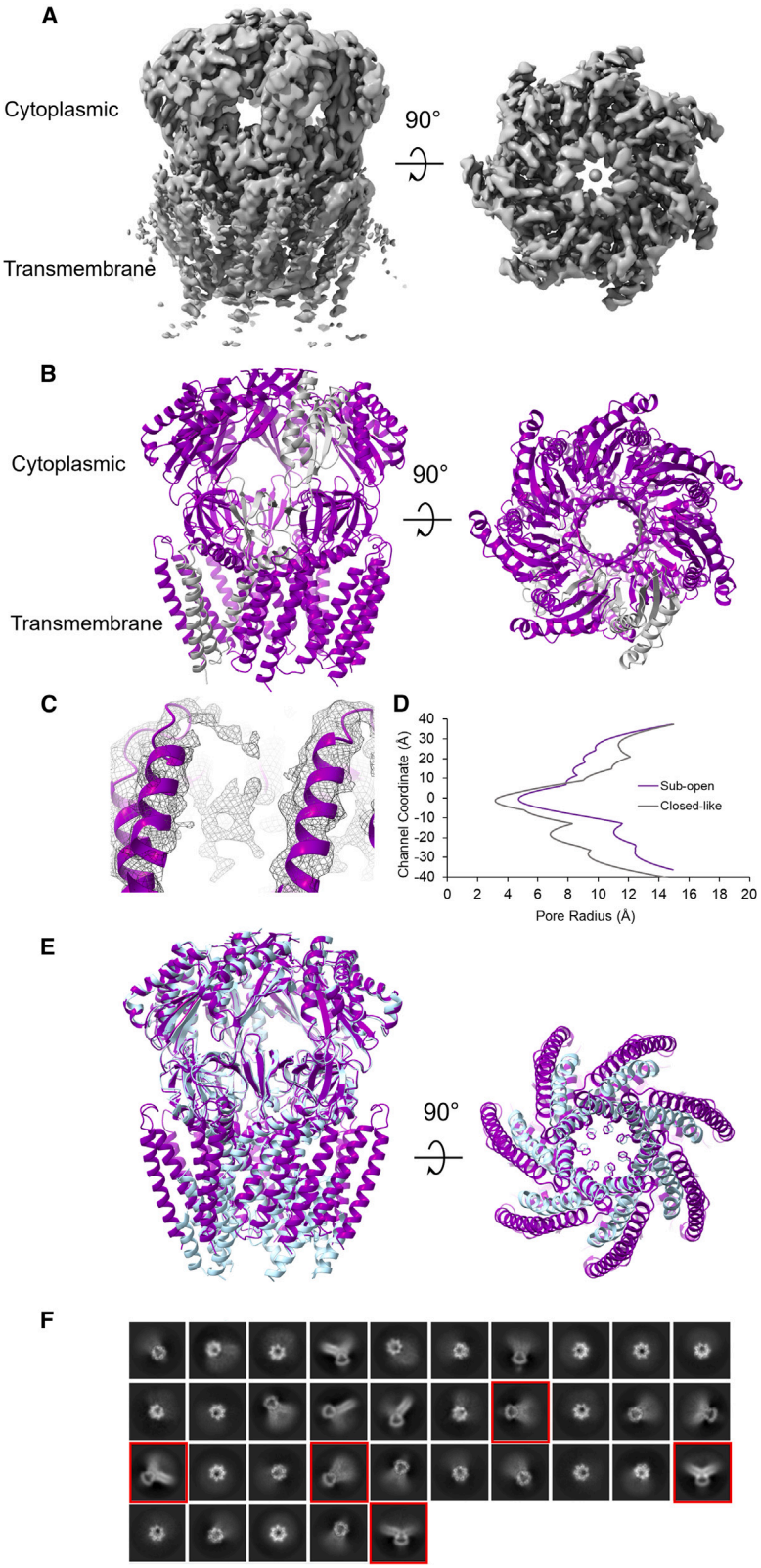

Figure 2. Cryo-EM structure of the heptameric YbiO channel in a sub-open state

(A) Coulomb potential map of YbiO with a global resolution of 3.15 Å viewed from the membrane plane and from the cytoplasmic side when rotated 90°.

(B) Overall model of YbiO shown in ribbons from the membrane plane and from the cytoplasmic side when rotated 90°. The YbiO monomer is colored in gray (PDB: 9GO3).

(C) Non-protein density between the TM helices of YbiO. The YbiO modeled TM helices are shown overlayed with the Coulomb potential map. Density in front and behind the non-protein density is cropped using the side view tool in ChimeraX[52] to allow visualization.

(D) HOLE analysis of the pores of the sub-open state in purple and the closed-like state (PDB: 7A46) in gray.

(E) Alignment of the YbiO model (this study, purple, PDB: 9GO3) with the published model (PDB: 7A46) of YbiO (light blue) from the side (left) and cytoplasmic view (right) to show the pore constricting residue (F553). The side view tool in UCSF Chimera[53] was used to remove the cytoplasmic domain and the ends of the TM helices to improve visualization.

(F) 2D classes show the dome-like indentation in the TM domain of YbiO and the change in the curvature of the TM domain. Classes showing different spacing between opposite sides of the TM domain are highlighted with red squares. These 2D classes are taken from a different data collection than the 3D reconstruction reported here. For this alternative data collection, YbiO was solubilized in LMNG/CHS (0.007%/0.0007%) detergent.

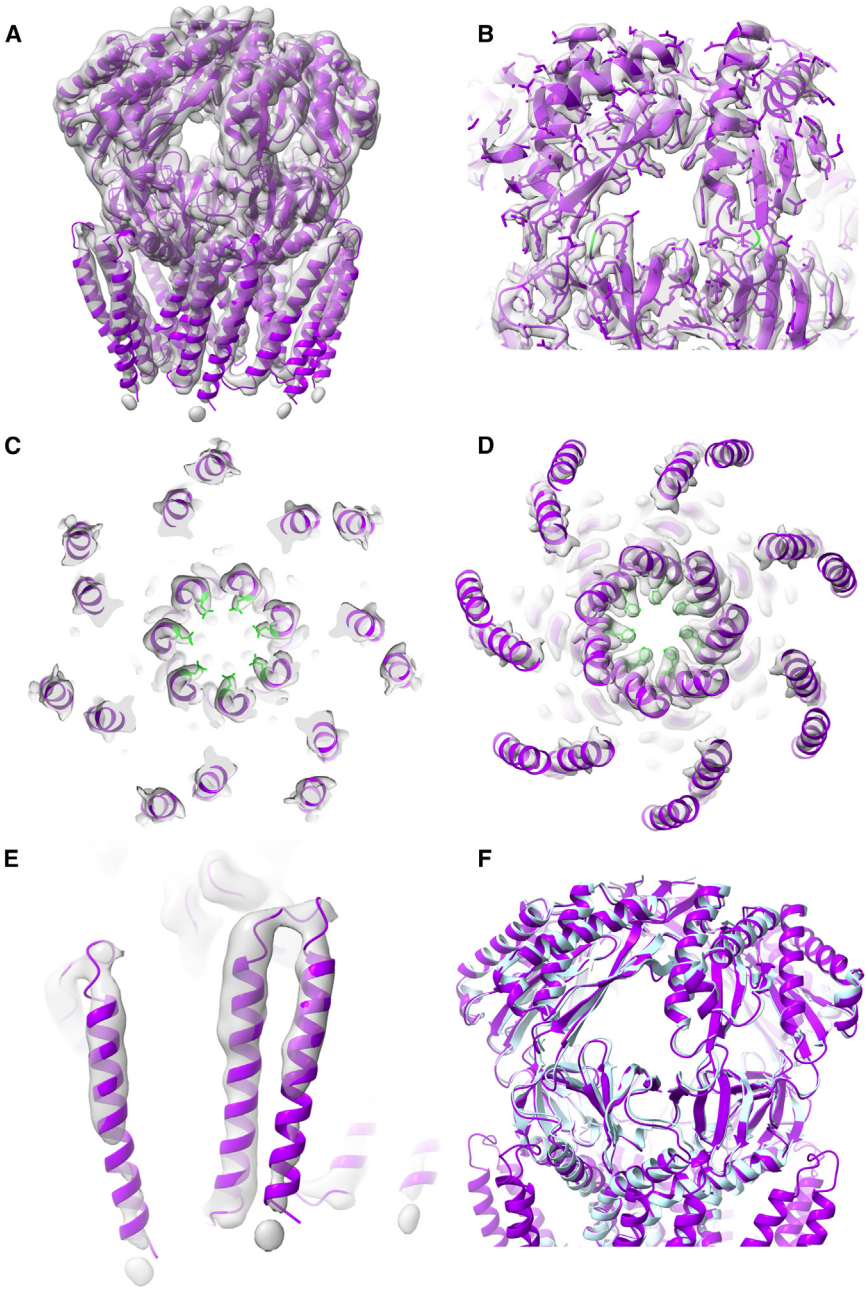

Figure 3. Structural analysis of the heptameric YbiO channel

(A) The built model (PDB: 9GO3) is superimposed with the unsharpened density map.

(B) A close-up of the cytoplasmic portal showing the location of G602R mutation. The model (PDB: 9GO3) is overlaid with the sharpened map and residue colored in lime green.

(C) Periplasmic view of YbiO shows residue L549 (lime green) with the model overlaid with the sharpened map. The side view tool in UCSF Chimera[53] was used to remove the cytoplasmic domain to improve visualization.

(D) Periplasmic view of YbiO showing the tightest constriction residue, F553 (lime green), with the model overlaid with the sharpened map. The side view tool in UCSF Chimera[53] was used to remove the cytoplasmic domain to improve visualization.

(E) TM1 and TM2 with connecting loop overlaid with the unsharpened map.

(F) Structural alignment of our sub-open structure (PDB: 9GO3) in purple with the closed-like structure of YbiO (PDB: 7A46) in light blue showing little global movements occur in the cytoplasmic domain when transitioning toward a more open state.

channel conductances seen for the largest gated pore to date, MscL. This unique functional behavior is unprecedented and has not been observed in any MscS-like family members of a similar size and architecture, including MscK and MscM. Our findings could now pave the way for further exploring the biophysical properties of other orthologous members in bacteria, plants, parasites, and fungi.[36,40,57,71] Potentially other larger members of the MscS-like family could also present larger conductances than previously seen in protoplasts, and systematic testing of purified channel proteins in GUVs would allow this to be demonstrated. When the unique biophysical properties of these large, gated pores are investigated and realized, they could then be exploited in biotechnological and antimicrobial applications, like MscL.[70]

Along with the large openings, we also observed two more dominant subconducting states, one of which is similar in its unitary to those recorded in protoplasts.[7,24] Subconducting states have been previously seen in MscS and MscL and are key to their mechanical sensing and response mechanisms.[7,23,46,49,50,72–74] It is therefore not unusual that we see multiple states present for YbiO. When protoplasts (or spheroplasts) are used in electrophysiology studies of *E. coli* MS channels, MscL is often used as a reference system. Therefore, fully open states of MscS-like channels, such as YbiO, may often be hindered or misidentified by the similar conductance of the MscL channel. Additionally, differences have been commonly seen in the electrophysiological profile and tension thresholds of other MS ion channels between spheroplasts and liposomes.[47,48] While Soy-PC GUVs are an established system for the electrophysiological characterization of mechanosensitive ion channels,[22,43–47] these lipids are different from those present in the cell membrane of *E. coli*. This could potentially affect the electrophysiological characteristics of YbiO, though this is unlikely to lead to the presence of larger openings exclusively in GUVs, since the same lipid system has been used by us for *E. coli* MscS here (Figure S1B) and in several other studies, and no higher than ~1 nS conductance has ever been reported.[43–47] Future work could use the MJF641 strain to confirm the presence of these large openings.[7]

While we expect lipid exchange from TM pockets to play a role in the mechanisms of these larger channels, this may also be associated with changes in membrane curvature. TMs 5–11 are a feature of the larger *E. coli* MscS-like members, and could potentially be involved in curvature sensing, a property which has been suggested for other MscS-like channels with additional TM helices. Substantial curvature changes in the TM domain of the protein are evidenced by our 2D classes for YbiO so it may be that this is a key characteristic of the larger MscS-like channels (Figure 2F). The overall architecture of the cytoplasmic domain appears to be conserved across the MscS-like family. The G602R mutation in *Salmonella* YbiO may be associated with increased pathogenicity of bacteria. The equivalent position in *E. coli* YbiO is G604. In the structure, this site sits on a loop across the cytoplasmic portals, and our structure reveals that is not altered during a transition from the closed-like to sub-open state, suggesting the pathogenicity effects observed may not be linked to channel gating, but local changes in the amino acid properties. These portals are associated with the regulation of ion selectivity and the regulation of conductance in MscS and other MscS-like channels.[25,57,74–76] Single-point mutations have been made in the cytoplasmic portal loop in FLYC1. Sequence alignments give no similarity but structurally one mutation is in a similar location to G604 in YbiO (K624E) and this mutation results in a remarkable 3-fold decrease in channel conductance.[57] The G604R mutation may alter the ion conductance properties, as it is likely that portals also form part of the permeation pathway in YbiO.

We believe our structure represents an intermediate state in the activation pathway of YbiO. In our structure, the channel adopts a sub-open conformation, with a larger pore diameter than the previously reported closed-like structure, which was able to conduct ions in computational electrophysiology experiments.[24] Membrane compression may be required to obtain a fully closed structure of a non-conducting YbiO, while mimicking tension conditions *in vitro* may be necessary to obtain larger opening forms of the channel. Indeed, recent studies showed that it is possible to mimic tension conditions within lipid scaffolds (i.e., nanodiscs and liposomes) using cyclodextrins, which induce controlled lipid depletion and stabilized functional states of MscS.[46,49,77] Structural analysis of MscS using electron paramagnetic resonance (EPR) spectroscopy and X-ray crystallography, demonstrated the channel is open in detergent,[78,79] while mostly closed in lipid membranes.[46,80] Other studies have suggested that in the closed state, the MscS channel pore may be occupied by lipids, and this may also be the case in the YbiO channel.[81–83] However, YbiO and MscS structures so far, except for one, have used detergent for extraction and this may remove lipids from the channel pore.[24,58,60,62,79,81,83,84] Future work could explore the use of extraction polymers for the structural characterization of the YbiO channels in a more native-like lipid environment.[83,85,86] Overall, the rotation of TM helices in the Flegler et al. structure (PDB: 7A46) indicates the structure was not fully closed,[24] and the ~2.8 Å increase in the pore diameter in our structure (PDB: 9GO3) compared to this, suggests that our structure resembles an intermediate substate, with pore dimensions consistent with the S_2 state reported here.

Despite recent advances in the structural determination of bacterial MS channels,[24,26,38] and successful monitoring of their cellular localization,[87] their functional roles remain poorly understood. The larger MscS-like channels may have subtler roles in osmoregulation, but additional functions are also likely.[12,14] Several of these channels have also been implicated in bacterial pathogenicity but the specific mechanisms for this are unknown.[14,17,71] Some MS channels have also been linked to biofilm formation, but this has not been fully investigated.[88,89] Further work using multidisciplinary approaches is needed to understand the functional roles, particularly of the larger members of the MscS-like superfamily in bacteria. To this end, our work sheds light on the unique biophysical properties of a large MscS-like channel representative, with equivalent pore openings to MscL, placing YbiO as one of the largest gated pores in nature. Our findings have direct implications for other members of the MscS-like family, which could be studied under a similar set-up to identify analogous or unique properties, paving the way for their biotechnological and antimicrobial exploitation.

RESOURCE AVAILABILITY

Lead contact

Further information and requests for resources and reagents should be directed to and will be fulfilled by the lead contact, Christos Pliotas (christos.pliotas@manchester.ac.uk).

Materials availability

All unique reagents generated in this study are available from the lead contact upon reasonable request.

Data and code availability

- The model coordinates for the cryo-EM structure of YbiO have been deposited in the Protein Data Bank (9GO3) and are publicly available from the data of publication. The associated maps are available from the Electron Microscopy Data Bank (EMD-51489) from the data of publication. The accession codes are also listed in the key resources table.
- The paper does not report any original code.
- Any additional information required to reanalyze the data reported is available from the lead contact upon request.

ACKNOWLEDGMENTS

This project was supported by a Biotechnology and Biological Sciences Research Council (BBSRC) grant (BB/S018069/1) to C.P., who also acknowledges support from the Wellcome Trust (WT) (219999/Z/19/Z) and the Chinese Scholarship Council (CSC) in the form of studentships for B.J.L. and N.Y respectively. CryoEM data were collected at the Astbury Biostructure Laboratory. The FEI Titan Krios microscopes were funded by the University of Leeds (UoL ABSL award) and Wellcome (108466/Z/15/Z), with the Falcon 4 and Selectris upgrades funded by Wellcome 221524/Z/20/Z. The Vitrobot was funded by Wellcome 218785/Z/19/Z. M.D. was funded by a BBSRC EU (Greece) partnering grant awarded to C.P. (BB/W018411/1). The Aston Institute for Membrane Excellence (AIME) is funded by UKRI's Research England as part of their Expanding Excellence in England (E3) fund. The authors acknowledge staff at the Astbury Biostructure Laboratory for technical support with cryo-EM data collection and for the running of facilities, and Antreas Kalli and Charline Fagnen for valuable discussions and support during the project. Graphical abstract created in BioRender. Ma, Y. (2025) https://BioRender.com/r95c891Biorender.

AUTHOR CONTRIBUTIONS

B.J.L., methodology, formal analysis, investigation, resources, data curation, writing – original draft, writing – review and editing, and visualization. M.D., validation, formal analysis, investigation, and writing – review and editing.

N.Y., validation, formal analysis, investigation, methodology, visualization, and writing – review and editing. J.D.L., validation, writing – review and editing, and supervision. S.P.M., validation, writing – review and editing, resources, and supervision. C.P., conceptualization, validation, resources, data curation, writing – original draft, writing – review and editing, supervision, project administration, and funding acquisition.

DECLARATION OF INTERESTS

The authors declare no competing interests.

STAR★METHODS

Detailed methods are provided in the online version of this paper and include the following:

- KEY RESOURCES TABLE
- EXPERIMENTAL MODEL AND STUDY PARTICIPANT DETAILS
- METHOD DETAILS
  - Protein expression
  - Protein purification
  - Cryo electron microscopy
  - Pore analysis using HOLE
  - Reconstitution into proteoliposomes
  - GUV formation and electrophysiology
- QUANTIFICATION AND STATISTICAL ANALYSIS

SUPPLEMENTAL INFORMATION

Supplemental information can be found online at https://doi.org/10.1016/j.str.2025.01.014.

Received: October 8, 2024
Revised: December 13, 2024
Accepted: January 13, 2025
Published: February 6, 2025

REFERENCES

1. Brohawn, S.G., Del Mármol, J., and MacKinnon, R. (2012). Crystal structure of the human K2P TRAAK, a lipid- and mechano-sensitive K+ ion channel. Science *335*, 436–441. https://doi.org/10.1126/science.1213808.
2. Kefauver, J.M., Ward, A.B., and Patapoutian, A. (2020). Discoveries in structure and physiology of mechanically activated ion channels. Nature *587*, 567–576. https://doi.org/10.1038/s41586-020-2933-1.
3. Laganowsky, A., Reading, E., Allison, T.M., Ulmschneider, M.B., Degiacomi, M.T., Baldwin, A.J., and Robinson, C.V. (2014). Membrane proteins bind lipids selectively to modulate their structure and function. Nature *510*, 172–175. https://doi.org/10.1038/nature13419.
4. Pliotas, C., Dahl, A.C.E., Rasmussen, T., Mahendran, K.R., Smith, T.K., Marius, P., Gault, J., Banda, T., Rasmussen, A., Miller, S., et al. (2015). The role of lipids in mechanosensation. Nat. Struct. Mol. Biol. *22*, 991–998. https://doi.org/10.1038/nsmb.3120.
5. Pliotas, C., and Naismith, J.H. (2017). Spectator no more, the role of the membrane in regulating ion channel function. Curr. Opin. Struct. Biol. *45*, 59–66. https://doi.org/10.1016/j.sbi.2016.10.017.
6. Schumann, U., Edwards, M.D., Rasmussen, T., Bartlett, W., van West, P., and Booth, I.R. (2010). YbdG in Escherichia coli is a threshold-setting mechanosensitive channel with MscM activity. Proc. Natl. Acad. Sci. USA *107*, 12664–12669. https://doi.org/10.1073/pnas.1001405107/.
7. Edwards, M.D., Black, S., Rasmussen, T., Rasmussen, A., Stokes, N.R., Stephen, T.L., Miller, S., and Booth, I.R. (2012). Characterization of three novel mechanosensitive channel activities in Escherichia coli. Channels *6*, 272–281. https://doi.org/10.4161/chan.20998.
8. Li, Y., Moe, P.C., Chandrasekaran, S., Booth, I.R., and Blount, P. (2002). Ionic regulation of MscK, a mechanosensitive channel from Escherichia coli. EMBO J. *21*, 5323–5330. https://doi.org/10.1093/emboj/cdf537.
9. Levina, N., To, S., Stokes, N.R., Louis, P., Jones, M.A., and Booth, I.R. (1999). Protection of Escherichia coli cells against extreme turgor by activation of MscS and MscL mechanosensitive channels: identification of genes required for MscS activity. EMBO J. *18*, 1730–1737. https://doi.org/10.1093/emboj/18.7.1730.
10. Booth, I.R. (2014). Bacterial mechanosensitive channels: progress towards an understanding of their roles in cell physiology. Curr. Opin. Microbiol. *18*, 16–22. https://doi.org/10.1016/j.mib.2014.01.005.
11. Kung, C., Martinac, B., and Sukharev, S. (2010). Mechanosensitive Channels in Microbes. Annu. Rev. Microbiol. *64*, 313–329. https://doi.org/10.1146/annurev.micro.112408.134106.
12. Rasmussen, T. (2016). How do mechanosensitive channels sense membrane tension? Biochem. Soc. Trans. *44*, 1019–1025. https://doi.org/10.1042/BST20160018.
13. Booth, I.R., and Blount, P. (2012). The MscS and MscL families of mechanosensitive channels act as microbial emergency release valves. J. Bacteriol. *194*, 4802–4809. https://doi.org/10.1128/JB.00576-12.
14. Sidarta, M., Baruah, L., and Wenzel, M. (2022). Roles of Bacterial Mechanosensitive Channels in Infection and Antibiotic Susceptibility. Pharmaceuticals *15*, 770. https://doi.org/10.3390/ph15070770.
15. Tan, M.-W., Rahme, L.G., Sternberg, J.A., Tompkins, R.G., and Ausubel, F.M. (1999). Pseudomonas aeruginosa killing of Caenorhabditis elegans used to identify P. aeruginosa virulence factors. Proc. Natl. Acad. Sci. USA *96*, 2408–2413. https://doi.org/10.1073/pnas.96.5.2408.
16. Chaudhuri, R.R., Morgan, E., Peters, S.E., Pleasance, S.J., Hudson, D.L., Davies, H.M., Wang, J., van Diemen, P.M., Buckley, A.M., Bowen, A.J., et al. (2013). Comprehensive Assignment of Roles for Salmonella Typhimurium Genes in Intestinal Colonization of Food-Producing Animals. PLoS Genet. *9*, e1003456. https://doi.org/10.1371/journal.pgen.1003456.
17. D'Alessandro, B., Escanda, V.P., Balestrazzi, L., Grattarola, F., Iriarte, A., Pickard, D., Yim, L., Chabalgoity, J.A., and Betancor, L. (2020). Comparative genomics of Salmonella enterica serovar Enteritidis ST-11 isolated in Uruguay reveals lineages associated with particular epidemiological traits. Sci. Rep. *10*, 1–8. https://doi.org/10.1038/s41598-020-60502-8.
18. Wang, Y., Jia, B., Xu, X., Zhang, L., Wei, C., Ou, H., Cui, Y., Shi, C., and Shi, X. (2018). Comparative genomic analysis and characterization of two Salmonella enterica serovar enteritidis isolates from poultry with notably different survival abilities in egg whites. Front. Microbiol. *9*, 2111. https://doi.org/10.3389/fmicb.2018.02111.
19. Kakuda, T., Koide, Y., Sakamoto, A., and Takai, S. (2012). Characterization of two putative mechanosensitive channel proteins of Campylobacter jejuni involved in protection against osmotic downshock. Vet. Microbiol. *160*, 53–60. https://doi.org/10.1016/j.vetmic.2012.04.044.
20. Wang, Z., Wang, X., Lu, P., Ni, C., Li, Y., and van der Veen, S. (2017). Identification and Characterization of the Neisseria Gonorrhoeae MscS-like Mechanosensitive Channel. Infect Immun *199*, 1–13. https://doi.org/10.1128/IAI.00090-18.
21. Bavi, N., Cox, C.D., Nikolaev, Y.A., and Martinac, B. (2023). Molecular insights into the force-from-lipids gating of mechanosensitive channels. Curr. Opin. Physiol. *36*, 100706. https://doi.org/10.1016/j.cophys.2023.100706.
22. Kapsalis, C., Wang, B., El Mkami, H., Pitt, S.J., Schnell, J.R., Smith, T.K., Lippiat, J.D., Bode, B.E., and Pliotas, C. (2019). Allosteric activation of an ion channel triggered by modification of mechanosensitive nano-pockets. Nat. Commun. *10*, 4619. https://doi.org/10.1038/s41467-019-12591-x.
23. Wang, B., Lane, B.J., Kapsalis, C., Ault, J.R., Sobott, F., El Mkami, H., Calabrese, A.N., Kalli, A.C., and Pliotas, C. (2022). Pocket delipidation induced by membrane tension or modification leads to a structurally analogous mechanosensitive channel state. Structure *30*, 608–622.e5. https://doi.org/10.1016/j.str.2021.12.004.

24. Flegler, V.J., Rasmussen, A., Rao, S., Wu, N., Zenobi, R., Sansom, M.S.P., Hedrich, R., Rasmussen, T., and Böttcher, B. (2020). The MscS-like channel YnaI has a gating mechanism based on flexible pore helices. Proc. Natl. Acad. Sci. USA *117*, 28754–28762. https://doi.org/10.1073/pnas.2005641117.

25. Li, Y., Hu, Y., Wang, J., Liu, X., Zhang, W., and Sun, L. (2020). Structural Insights into a Plant Mechanosensitive Ion Channel MSL1. Cell Rep. *30*, 4518–4527.e3. https://doi.org/10.1016/j.celrep.2020.03.026.

26. Mount, J., Maksaev, G., Summers, B.T., Fitzpatrick, J.A.J., and Yuan, P. (2022). Structural basis for mechanotransduction in a potassium-dependent mechanosensitive ion channel. Nat. Commun. *13*, 6904. https://doi.org/10.1038/s41467-022-34737-0.

27. Procko, C., Murthy, S., Keenan, W.T., Mousavi, S.A.R., Dabi, T., Coombs, A., Procko, E., Baird, L., Patapoutian, A., and Chory, J. (2021). Stretch-activated ion channels identified in the touch-sensitive structures of carnivorous droseraceae plants. Elife *10*, e64250. https://doi.org/10.7554/eLife.64250.

28. Zhang, J., Maksaev, G., and Yuan, P. (2023). Open structure and gating of the Arabidopsis mechanosensitive ion channel MSL10. Nat. Commun. *14*, 6284. https://doi.org/10.1038/s41467-023-42117-5.

29. Typas, A., Becker, G., and Hengge, R. (2007). The molecular basis of selective promoter activation by the σs subunit of RNA polymerase. Mol. Microbiol. *63*, 1296–1306. https://doi.org/10.1111/j.1365-2958.2007.05601.x.

30. Stokes, N.R., Murray, H.D., Subramaniam, C., Gourse, R.L., Louis, P., Bartlett, W., Miller, S., and Booth, I.R. (2003). A role for mechanosensitive channels in survival of stationary phase: Regulation of channel expression by RpoS. Proc. Natl. Acad. Sci. USA *100*, 15959–15964.

31. Hengge, R. (2009). Proteolysis of σS (RpoS) and the general stress response in Escherichia coli. Res. Microbiol. *160*, 667–676. https://doi.org/10.1016/j.resmic.2009.08.014.

32. McLaggan, D., Jones, M.A., Gouesbet, G., Levina, N., Lindey, S., Epstein, W., and Booth, I.R. (2002). Analysis of the kefA2 mutation suggests that KefA is a cation-specific channel involved in osmotic adaptation in Escherichia coli. Mol. Microbiol. *43*, 521–536. https://doi.org/10.1046/j.1365-2958.2002.02764.x.

33. Li, C., Edwards, M.D., Jeong, H., Roth, J., and Booth, I.R. (2007). Identification of mutations that alter the gating of the Escherichia coli mechanosensitive channel protein, MscK. Mol. Microbiol. *64*, 560–574. https://doi.org/10.1111/j.1365-2958.2007.05672.x.

34. Gustin, M.C., Zhou, X.L., Martinac, B., and Kung, C. (1988). A Mechanosensitive Ion Channel in the Yeast Plasma Membrane. Science *242*, 762–765. https://doi.org/10.1126/SCIENCE.2460920.

35. Nakayama, Y., Yoshimura, K., and Iida, H. (2012). Organellar mechanosensitive channels in fission yeast regulate the hypo-osmotic shock response. Nat. Commun. *3*, 1020. https://doi.org/10.1038/ncomms2014.

36. Dionysopoulou, M., Yan, N., Wang, B., Pliotas, C., and Diallinas, G. (2022). Genetic and cellular characterization of MscS-like putative channels in the filamentous fungus Aspergillus nidulans. Channels *16*, 148–158. https://doi.org/10.1080/19336950.2022.2098661.

37. Deng, Z., Maksaev, G., Schlegel, A.M., Zhang, J., Rau, M., Fitzpatrick, J.A.J., Haswell, E.S., and Yuan, P. (2020). Structural mechanism for gating of a eukaryotic mechanosensitive channel of small conductance. Nat. Commun. *11*, 3690. https://doi.org/10.1038/s41467-020-17538-1.

38. Hu, W., Wang, Z., and Zheng, H. (2021). Mechanosensitive channel YnaI has lipid-bound extended sensor paddles. Commun. Biol. *4*, 602. https://doi.org/10.1038/s42003-021-02122-0.

39. Jumper, J., Evans, R., Pritzel, A., Green, T., Figurnov, M., Ronneberger, O., Tunyasuvunakool, K., Bates, R., Žídek, A., Potapenko, A., et al. (2021). Highly accurate protein structure prediction with AlphaFold. Nature *596*, 583–589. https://doi.org/10.1038/s41586-021-03819-2.

40. Basu, D., and Haswell, E.S. (2020). The Mechanosensitive Ion Channel MSL10 Potentiates Responses to Cell Swelling in Arabidopsis Seedlings. Curr. Biol. *30*, 2716–2728.e6. https://doi.org/10.1016/J.CUB.2020.05.015.

41. Basu, D., Shoots, J.M., and Haswell, E.S. (2020). Interactions between the N- and C-termini of the mechanosensitive ion channel AtMSL10 are consistent with a three-step mechanism for activation. J. Exp. Bot. *71*, 4020–4032. https://doi.org/10.1093/JXB/ERAA192.

42. Hamilton, E.S., and Haswell, E.S. (2017). The Tension-sensitive Ion Transport Activity of MSL8 is Critical for its Function in Pollen Hydration and Germination. Plant Cell Physiol. *58*, 1222–1237. https://doi.org/10.1093/pcp/pcw230.

43. Sukharev, S. (2002). Purification of the Small Mechanosensitive Channel of Escherichia coli (MscS): the Subunit Structure, Conduction, and Gating Characteristics in Liposomes. Biophys. J. *83*, 290–298. https://doi.org/10.1016/S0006-3495(02)75169-2.

44. Rasmussen, T., Rasmussen, A., Singh, S., Galbiati, H., Edwards, M.D., Miller, S., and Booth, I.R. (2015). Properties of the Mechanosensitive Channel MscS Pore Revealed by Tryptophan Scanning Mutagenesis. Biochemistry *54*, 4519–4530. https://doi.org/10.1021/acs.biochem.5b00294.

45. Mukherjee, N., Jose, M.D., Birkner, J.P., Walko, M., Ingólfsson, H.I., Dimitrova, A., Arnarez, C., Marrink, S.J., and Koçer, A. (2014). The activation mode of the mechanosensitive ion channel, MscL, by lysophosphatidylcholine differs from tension-induced gating. FASEB (Fed. Am. Soc. Exp. Biol.) J. *28*, 4292–4302. https://doi.org/10.1096/fj.14-251579.

46. Lane, B.J., Ma, Y., Yan, N., Wang, B., Ackermann, K., Karamanos, T.K., Bode, B.E., and Pliotas, C. (2024). Monitoring the conformational ensemble and lipid environment of a mechanosensitive channel under cyclodextrin-induced membrane tension. Structure *32*, 739–750.e4. https://doi.org/10.1016/j.str.2024.02.020.

47. Nomura, T., Cranfield, C.G., Deplazes, E., Owen, D.M., Macmillan, A., Battle, A.R., Constantine, M., Sokabe, M., and Martinac, B. (2012). Differential effects of lipids and lyso-lipids on the mechanosensitivity of the mechanosensitive channels MscL and MscS. Proc. Natl. Acad. Sci. USA *109*, 8770–8775. https://doi.org/10.1073/pnas.1200051109.

48. Malcolm, H.R., Blount, P., and Maurer, J.A. (2015). The mechanosensitive channel of small conductance (MscS) functions as a Jack-In-The Box. Biochim. Biophys. Acta *1848*, 159–166. https://doi.org/10.1016/j.bbamem.2014.10.022.

49. Zhang, Y., Daday, C., Gu, R.-X., Cox, C.D., Martinac, B., de Groot, B.L., and Walz, T. (2021). Visualization of the mechanosensitive ion channel MscS under membrane tension. Nature *590*, 509–514. https://doi.org/10.1038/s41586-021-03196-w.

50. Konijnenberg, A., Yilmaz, D., Ingólfsson, H.I., Dimitrova, A., Marrink, S.J., Li, Z., Venien-Bryan, C., Sobott, F., and Kocer, A. (2020). Global structural changes of an ion channel during its gating are followed by ion mobility mass spectrometry. Proc. Natl. Acad. Sci. USA *111*, 17170–17175. https://doi.org/10.1073/pnas.1413118111.

51. Sukharev, S., Betanzos, M., Chiang, C.-S., and Guy, H.R. (2001). The gating mechanism of the large mechanosensitive channel MscL. Nature *409*, 720–724. https://doi.org/10.1038/35055559.

52. Pettersen, E.F., Goddard, T.D., Huang, C.C., Meng, E.C., Couch, G.S., Croll, T.I., Morris, J.H., and Ferrin, T.E. (2021). UCSF ChimeraX: Structure visualization for researchers, educators, and developers. Protein Sci. *30*, 70–82. https://doi.org/10.1002/pro.3943.

53. Pettersen, E.F., Goddard, T.D., Huang, C.C., Couch, G.S., Greenblatt, D.M., Meng, E.C., and Ferrin, T.E. (2004). UCSF Chimera—A Visualization System for Exploratory Research and Analysis. J. Comput. Chem. *25*, 1605–1612. https://doi.org/10.1002/jcc.20084.

54. Catalano, C., Ben-Hail, D., Qiu, W., Blount, P., des Georges, A., and Guo, Y. (2021). Cryo-EM Structure of Mechanosensitive Channel Ynai Using SMA2000: Challenges and Opportunities. Membranes *11*, 849. https://doi.org/10.3390/membranes11110849.

55. Smart, O.S., Neduvelil, J.G., Wang, X., Wallace, B.A., and Sansom, M.S. (1996). HOLE: A program for the analysis of the pore dimensions of ion

channel structural models. J. Mol. Graph. *14*, 354–376. https://doi.org/10.1016/S0263-7855(97)00009-X.

56. Klesse, G., Rao, S., Sansom, M.S.P., and Tucker, S.J. (2019). CHAP: A Versatile Tool for the Structural and Functional Annotation of Ion Channel Pores. J. Mol. Biol. *431*, 3353–3365. https://doi.org/10.1016/j.jmb.2019.06.003.

57. Jojoa-Cruz, S., Saotome, K., Tsui, C.C.A., Lee, W.H., Sansom, M.S.P., Murthy, S.E., Patapoutian, A., and Ward, A.B. (2022). Structural insights into the Venus flytrap mechanosensitive ion channel Flycatcher1. Nat. Commun. *13*, 850. https://doi.org/10.1038/s41467-022-28511-5.

58. Steinbacher, S., Bass, R., Strop, P., and Rees, D.C. (2007). Structures of the Prokaryotic Mechanosensitive Channels MscL and MscS. Curr. Top. Membr. *58*, 1–24. https://doi.org/10.1016/S1063-5823(06)58001-9.

59. Cruickshank, C.C., Minchin, R.F., Le Dain, A.C., and Martinac, B. (1997). Estimation of the Pore Size of the Large-Conductance Mechanosensitive Ion Channel of Escherichia coli. Biophys. J. *73*, 1925–1931. https://doi.org/10.1016/S0006-3495(97)78223-7.

60. Bass, R.B., Strop, P., Barclay, M., and Rees, D.C. (2002). Crystal Structure of Escherichia coli MscS, a Voltage-Modulated and Mechanosensitive Channel. Science *298*, 1582–1587. https://doi.org/10.1126/science.1077945.

61. Böttcher, B., Prazak, V., Rasmussen, A., Black, S.S., and Rasmussen, T. (2015). The Structure of YnaI Implies Structural and Mechanistic Conservation in the MscS Family of Mechanosensitive Channels. Structure *23*, 1705–1714. https://doi.org/10.1016/j.str.2015.06.023.

62. Wang, W., Black, S.S., Edwards, M.D., Miller, S., Morrison, E.L., Bartlett, W., Dong, C., Naismith, J.H., and Booth, I.R. (2008). The structure of an open form of an E. coli mechanosensitive channel at 3.45 Å resolution. Science *321*, 1179–1183. https://doi.org/10.1126/science.1159262.

63. Guo, Y.R., and Mackinnon, R. (2017). Structure-based membrane dome mechanism for Piezo mechanosensitivity. Elife *6*, 1–19. https://doi.org/10.7554/eLife.33660.

64. Wang, L., Zhou, H., Zhang, M., Liu, W., Deng, T., Zhao, Q., Li, Y., Lei, J., Li, X., and Xiao, B. (2019). Structure and mechanogating of the mammalian tactile channel PIEZO2. Nature *573*, 225–229. https://doi.org/10.1038/s41586-019-1505-8.

65. Zhao, Q., Zhou, H., Chi, S., Wang, Y., Wang, J., Geng, J., Wu, K., Liu, W., Zhang, T., Dong, M.Q., et al. (2018). Structure and mechanogating mechanism of the Piezo1 channel. Nature *554*, 487–492. https://doi.org/10.1038/nature25743.

66. Yang, X., Lin, C., Chen, X., Li, S., Li, X., and Xiao, B. (2022). Structure deformation and curvature sensing of PIEZO1 in lipid membranes. Nature *604*, 377–383. https://doi.org/10.1038/s41586-022-04574-8.

67. Kapsalis, C., Ma, Y., Bode, B.E., and Pliotas, C. (2020). In-lipid structure of pressure sensitive domains hints mechanosensitive channel functional diversity. Biophys. J. *119*, 448–459. https://doi.org/10.1016/j.bpj.2020.06.012.

68. Park, Y.C., Reddy, B., Bavi, N., Perozo, E., and Faraldo-Gómez, J.D. (2023). State-specific morphological deformations of the lipid bilayer explain mechanosensitive gating of MscS ion channels. Elife *12*, e81445. https://doi.org/10.7554/eLife.81445.

69. Doerner, J.F., Febvay, S., and Clapham, D.E. (2012). Controlled delivery of bioactive molecules into live cells using the bacterial mechanosensitive channel MscL. Nat. Commun. *3*, 990. https://doi.org/10.1038/ncomms1999.

70. Lane, B.J., and Pliotas, C. (2023). Approaches for the modulation of mechanosensitive MscL channel pores. Front. Chem. *11*, 1162412. https://doi.org/10.3389/fchem.2023.1162412.

71. Dave, N., Cetiner, U., Arroyo, D., Fonbuena, J., Tiwari, M., Barrera, P., Lander, N., Anishkin, A., Sukharev, S., and Jimenez, V. (2021). A novel mechanosensitive channel controls osmoregulation, differentiation, and infectivity in trypanosoma cruzi. Elife *10*, e67449. https://doi.org/10.7554/ELIFE.67449.

72. Betanzos, M., Chiang, C.S., Guy, H.R., and Sukharev, S. (2002). A large iris-like expansion of a mechanosensitive channel protein induced by membrane tension. Nat. Struct. Biol. *9*, 704–710. https://doi.org/10.1038/nsb828.

73. Boucher, P.A., Morris, C.E., and Joós, B. (2009). Mechanosensitive Closed-Closed Transitions in Large Membrane Proteins: Osmoprotection and Tension Damping. Biophys. J. *97*, 2761–2770. https://doi.org/10.1016/j.bpj.2009.08.054.

74. Cox, C.D., Nomura, T., Ziegler, C.S., Campbell, A.K., Wann, K.T., and Martinac, B. (2013). Selectivity mechanism of the mechanosensitive channel MscS revealed by probing channel subconducting states. Nat. Commun. *4*, 2137. https://doi.org/10.1038/ncomms3137.

75. Gamini, R., Sotomayor, M., Chipot, C., and Schulten, K. (2011). Cytoplasmic domain filter function in the mechanosensitive channel of small conductance. Biophys. J. *101*, 80–89. https://doi.org/10.1016/j.bpj.2011.05.042.

76. Zhang, X., Wang, J., Feng, Y., Ge, J., Li, W., Sun, W., Iscla, I., Yu, J., Blount, P., Li, Y., and Yang, M. (2012). Structure and molecular mechanism of an anion-selective mechanosensitive channel of small conductance. Proc. Natl. Acad. Sci. USA *109*, 18180–18185. https://doi.org/10.1073/pnas.1207977109.

77. Cox, C.D., Zhang, Y., Zhou, Z., Walz, T., and Martinac, B. (2021). Cyclodextrins increase membrane tension and are universal activators of mechanosensitive channels. Proc. Natl. Acad. Sci. USA *118*, e2104820118. https://doi.org/10.1073/pnas.2104820118.

78. Pliotas, C., Ward, R., Branigan, E., Rasmussen, A., Hagelueken, G., Huang, H., Black, S.S., Booth, I.R., Schiemann, O., and Naismith, J.H. (2012). Conformational state of the MscS mechanosensitive channel in solution revealed by pulsed electron-electron double resonance (PELDOR) spectroscopy. Proc. Natl. Acad. Sci. USA *109*, 2675–2682. https://doi.org/10.1073/pnas.1202286109.

79. Lai, J.Y., Poon, Y.S., Kaiser, J.T., and Rees, D.C. (2013). Open and shut: Crystal structures of the dodecylmaltoside solubilized mechanosensitive channel of small conductance from Escherichia coli and Helicobacter pylori at 4.4 Å and 4.1 Å resolutions. Protein Sci. *22*, 502–509. https://doi.org/10.1002/pro.2222.

80. Ward, R., Pliotas, C., Branigan, E., Hacker, C., Rasmussen, A., Hagelueken, G., Booth, I.R., Miller, S., Lucocq, J., Naismith, J.H., and Schiemann, O. (2014). Probing the Structure of the Mechanosensitive Channel of Small Conductance in Lipid Bilayers with Pulsed Electron-Electron Double Resonance. Biophys. J. *106*, 834–842. https://doi.org/10.1016/j.bpj.2014.01.008.

81. Reddy, B., Bavi, N., Lu, A., Park, Y., and Perozo, E. (2019). Molecular basis of force-from-lipids gating in the mechanosensitive channel mscs. Elife *8*, e50486. https://doi.org/10.7554/eLife.50486.

82. Flegler, V.J., Rasmussen, A., Borbil, K., Boten, L., Chen, H.A., Deinlein, H., Halang, J., Hellmanzik, K., Löffler, J., Schmidt, V., et al. (2021). Mechanosensitive channel gating by delipidation. Proc. Natl. Acad. Sci. USA *118*, e2107095118. https://doi.org/10.1073/pnas.2107095118.

83. Moller, E., Britt, M., Zhou, F., Yang, H., Anshkin, A., Ernst, R., Sukharev, S., and Matthies, D. (2024). Polymer-extracted structure of the mechanosensitive channel MscS reveals the role of protein-lipid interactions in the gating cycle. Preprint at bioRxiv. https://doi.org/10.1101/2024.01.22.576751.

84. Rasmussen, T., Flegler, V.J., Rasmussen, A., and Böttcher, B. (2019). Structure of the Mechanosensitive Channel MscS Embedded in the Membrane Bilayer. J. Mol. Biol. *431*, 3081–3090. https://doi.org/10.1016/j.jmb.2019.07.006.

85. Unger, L., Ronco-Campaña, A., Kitchen, P., Bill, R.M., and Rothnie, A.J. (2021). Biological insights from SMA-extracted proteins. Biochem. Soc. Trans. *49*, 1349–1359. https://doi.org/10.1042/BST20201067.

86. Guo, Y. (2021). Detergent-free systems for structural studies of membrane proteins. Biochem. Soc. Trans. *49*, 1361–1374. https://doi.org/10.1042/BST20201080.

87. Van Den Berg, J., Galbiati, H., Rasmussen, A., Miller, S., and Poolman, B. (2016). On the mobility, membrane location and functionality of mechanosensitive channels in Escherichia coli. Sci. Rep. *6*, 32709. https://doi.org/10.1038/srep32709.

88. Carniello, V., Peterson, B.W., van der Mei, H.C., and Busscher, H.J. (2020). Role of adhesion forces in mechanosensitive channel gating in Staphylococcus aureus adhering to surfaces. NPJ Biofilms Microbiomes *6*, 31. https://doi.org/10.1038/s41522-020-00141-z.

89. O'Loughlin, C.T., Miller, L.C., Siryaporn, A., Drescher, K., Semmelhack, M.F., and Bassler, B.L. (2013). A quorum-sensing inhibitor blocks Pseudomonas aeruginosa virulence and biofilm formation. Proc. Natl. Acad. Sci. USA *110*, 17981–17986. https://doi.org/10.1073/pnas.1316981110.

90. Scheres, S.H.W. (2012). RELION: Implementation of a Bayesian approach to cryo-EM structure determination. J. Struct. Biol. *180*, 519–530. https://doi.org/10.1016/j.jsb.2012.09.006.

91. Zivanov, J., Nakane, T., Forsberg, B.O., Kimanius, D., Hagen, W.J., Lindahl, E., and Scheres, S.H. (2018). New tools for automated high-resolution cryo-EM structure determination in RELION-3. Elife *7*, e42166. https://doi.org/10.7554/eLife.42166.001.

92. Zheng, S.Q., Palovcak, E., Armache, J.P., Verba, K.A., Cheng, Y., and Agard, D.A. (2017). MotionCor2: Anisotropic Correction of Beam-Induced Motion for Improved Cryo-Electron Microscopy (Nature Publishing Group). https://doi.org/10.1038/nmeth.4193.

93. Rohou, A., and Grigorieff, N. (2015). CTFFIND4: Fast and accurate defocus estimation from electron micrographs. J. Struct. Biol. *192*, 216–221. https://doi.org/10.1016/j.jsb.2015.08.008.

94. Wagner, T., Merino, F., Stabrin, M., Moriya, T., Antoni, C., Apelbaum, A., Hagel, P., Sitsel, O., Raisch, T., Prumbaum, D., et al. (2019). SPHIRE-crYOLO is a fast and accurate fully automated particle picker for cryo-EM. Commun. Biol. *2*, 218. https://doi.org/10.1038/s42003-019-0437-z.

95. Punjani, A., Rubinstein, J.L., Fleet, D.J., and Brubaker, M.A. (2017). CryoSPARC: Algorithms for rapid unsupervised cryo-EM structure determination. Nat. Methods *14*, 290–296. https://doi.org/10.1038/nmeth.4169.

CellPress
OPEN ACCESS

STAR★METHODS

KEY RESOURCES TABLE

REAGENT or RESOURCE	SOURCE	IDENTIFIER
Bacterial and virus strains		
MJF612 *E. coli* strain	Levina et al.[9] Edwards et al.[7]	N/A
Chemicals, peptides, and recombinant proteins		
N-Dodecyl-b-D-Maltopyranoside (DDM), anagrade	Anatrace or Glycon	Cat# D310 or D97002
Glyco-diosgenin (GDN)	Anatrace	Cat# GDN101
Lauryl Maltose Neopentyl Glycol (LMNG)	Anatrace	Cat# NG310
Cholesteryl Hemisuccinate Tris Salt (CHS)	Anatrace	Cat# CH210
Soy L-α-phosphatidylcholine (Soy-PC)	Anatrace	Cat# 441601
Deposited data		
Atomic coordinates and structural factors: YbiO	This study	PDB: 9GO3
CryoEM map	This study	EMDB: 51489
Atomic coordinates and structural factors: closed-like YbiO	Flegler et al.[24]	PDB: 7A46
Atomic coordinates and structural factors: closed MscS	Steinbacher et al.[58]	PDB: 2OAU
Atomic coordinates and structural factors: closed MscS	Zhang et al.[49]	PDB: 6VYK
Recombinant DNA		
Plasmid: pTrcYbiOxHis6 plasmid	Edwards et al.[7]	N/A
Software and algorithms		
Relion 3.1	Zivanov et al.[90,91]	https://relion.readthedocs.io/en/release-3.1/Installation.html
MotionCor2	Zheng et al.[92]	N/A
CtfFind	Rohou et al.[93]	N/A
CrYOLO 1.5.6	Wagner et al.[94]	https://cryolo.readthedocs.io/en/stable/installation.html
CryoSPARC 3.1.1	Punjani et al.[95]	https://cryosparc.com/docs
HOLE	Smart et al.[55]	https://www.holeprogram.org/
pClamp 10	Molecular Devices	https://support.moleculardevices.com/s/article/Axon-pCLAMP-10-Electrophysiology-Data-Acquisition-Analysis-Software-Download-Page
Other		
Proteus X-spinner 2.5 PES membrane, (100 kDa MWCO)	Molecular Dimensions	Cat# PAL-X-100-24
Ni-NTA Agarose Resin	Invitrogen	Cat# R901-15
Superose 6 Increase 10/300 GL column	Cytiva	Cat# 29091596

EXPERIMENTAL MODEL AND STUDY PARTICIPANT DETAILS

Plasmid propagation was performed using DH5α competent *E. coli* cells plated on Luria Broth (LB) agar (37°C) or inoculated in LB liquid media (37°C, 200 RPM); both grown overnight in the presence of a selective antibiotic. Recombinant *E. coli* YbiO was produced in *E. coli* MJF612 cultured in LB Broth supplemented with selective antibiotic overnight (25°C, 200 RPM) following IPTG induction (final concentration 0.8 mM) at an OD600 ~0.8. Full details are available in the STAR Methods text.

METHOD DETAILS

Protein expression

The pTrcYbiOH6 plasmid was used for expression. The plasmid was transformed into chemically competent MJF612 *E. coli* cells. 3 × 50 mL falcon tube containing ~12 mL of LB media was inoculated with a single MJF612 colony or glycerol stock containing the pTrcYbiOH6 WT or mutant plasmid and grown overnight at 37°C, 180 rpm. 17 mL of overnight culture was added to 2 × 2 L pre-culture flasks containing 500 mL LB media and incubated at 37°C, 180 rpm. The pre-cultures were grown to an OD600 of 0.6, then 50 mL was taken from the cultures and placed into 16 × 2 L flasks containing 500 mL and incubated at 37°C, 180 rpm. The bacteria were then grown to an OD600 of 0.8, induced with 0.8 mM IPTG and then incubated overnight at 30°C, 180 rpm. Cells were harvested by centrifugation at 5000 × g and stored at -80°C, until further use.

Protein purification

Following protein expression, cell pellets were resuspended in phosphate-buffered saline and subjected to lysis using a cell disrupter at 30 kpsi. To remove cell debris the suspension was centrifuged at 5000 × g for 1 hr and the resulting supernatant was centrifuged again at 100,000 × g for 1 h. The membrane pellet was resuspended and solubilized in a buffer containing 50 mM sodium phosphate at pH 7.5, 300 mM NaCl, 10% v/v glycerol, 20 mM imidazole, and 1.0% w/v DDM and incubated at 4°C for 1 h. The sample was then centrifuged at 100,000 × g for 20 min in an ultracentrifuge to remove insoluble contaminants. The supernatant was passed through a Ni^{2+}-NTA column containing 1 mL of Ni^{2+}-NTA beads. The column was then washed with 15 mL wash buffer containing 50 mM sodium phosphate at pH 7.5, 300 mM NaCl, 25 mM imidazole and detergent (0.021% GDN/0.0021% CHS). The protein was then eluted from the column with 6 mL of wash buffer supplemented with 300 mM imidazole. Finally, the protein was subjected to SEC using a Superose 6 Increase 10/300 column (GE Healthcare) equilibrated with a buffer containing 50 mM sodium phosphate pH 7.5, 300 mM NaCl and detergent (0.021% GDN/0.0021% CHS). For the generation of the 2D classes reported in Figure 2F, the same process was followed with the exception that YbiO was solubilised in 0.007%/0.0007% LMNG/CHS. CHS is a cholesterol analogue, and the bacterial cell membrane does not contain cholesterol-like lipids. We looked at the addition of CHS because it is often paired with LMNG and GDN in structural cryoEM studies and it appeared to increase the stability and homogeneity of the YbiO sample.

Cryo electron microscopy

For 3D structural determination of YbiO, 1.2/1.3 carbon Quantifoils and 1.2/1.3 UltrAuFoil were glow discharged using a Cressington 208 glow discharger. The YbiO protein sample (1-1.2 mg/mL) in a buffer (50 mM Na-phosphate buffer pH 7.5, 300 mM NaCl pH 7.5, detergent) was added to grids in the humidity chamber of the Vitrobot. The vitroblot blotted the grids with a blotting force of 6 and a blot time of 3 sec and transferred the grid into liquid ethane. The grid was quickly transferred from ethane to liquid nitrogen and into a puc for storage. An FEI Titan Krios with a Falcon IV and Selectris energy filter, or a Gatan K2 direct electron detector (ABSL, University of Leeds) were used for screening and data acquisition. Data were collected at 300 kV with a pixel size of 0.74. Motion correction and CTF estimation were done on-the-fly using the RELION 3.1 implementation of MotionCor2 and CtfFind.[90–93] CrYOLO 1.5.6 was used for particle picking using a trained model for my particles and particles were imported into RELION 3.1 for extraction.[94] Extracted particles were imported into CryoSPARC 3.1.1 for the remainder of the image processing pipelines.[95] C7 symmetry was used for 3D refinement. An overview of the processing pipeline is shown in Figure S6. For the generation of the 2D classes reported in Figure 2F, the same process was followed with the exception that YbiO was solubilised in 0.007%/0.0007% LMNG/CHS.

Pore analysis using HOLE

The pore diameter along the channel axis for ion channel structures was determined using HOLE.[55] Coordinates for the Cα carbon of the constricting residue on each of the chains were averaged for use as the cpoint in HOLE, a central starting point in the channel for analysis. The constricting residue with the smallest pore diameter was used as the cpoint. The constricting residue was F553 for YbiO. A simple.rad radius file was used for specifying the Van der Waals radii for each atom.

Reconstitution into proteoliposomes

Protocols for the reconstitution of MS channels (i.e. YbiO and MscS) in liposomes followed here, were previously described.[22,46] In brief, 200 μL of a 10 mg/mL 20% Soy PC (Avanti) stock dissolved in chloroform was dried in a small glass vial under nitrogen flow. While drying the lipids, the vial was slowly rotated until a thin lipid layer film was formed. 500 μL of lipid buffer (containing 50 mM sodium phosphate buffer of pH 7.5 and 300 mM NaCl) was added into the vial, and the mixture was sonicated for 30 min until the solution was transparent. After addition of DDM at a final concentration of 0.02%, purified protein samples and liposome solutions were mixed in a weight ratio (1:150) at RT for 1 h. Lipid buffer was left incubating with 300 mg of prewetted Bio-beads (Bio-Rad) at 4°C overnight. After removal of Bio-beads, the mixture was centrifuged at 100,000 × g for 1 h. The resulting proteoliposome pellets were resuspended in 80 μL of lipid buffer, flash frozen in liquid-N_2 in 10 μL aliquots and stored at -80°C for future use.

GUV formation and electrophysiology

Detailed protocols have been previously described here.[22,46] Briefly, proteoliposome were formed and pelleted. For the YbiO only experiments the protein:lipid molar ratio was 1:50. Pellet aliquots were thawed at RT, one day before the recordings, dehydrated overnight in a desiccator at 4°C and then rehydrated for 2 h at RT in rehydration buffer (50 mM sodium phosphate buffer pH 7.5,

300 mM NaCl, and 400 mM sucrose). 5 μL of the buffer containing GUVs was added to the centre of a small petri dish (containing 2.5 mL of working solution: 5 mM HEPES pH 7.2, adjusted with KOH, 200 mM KCl, and 40 mM $MgCl_2$). Proteoliposomes were subsequently collapsed in working solution and formed new giant blisters. Symmetrical ionic solutions were used in all recordings. Patch pipettes were pulled from thick-walled borosilicate glass capillaries (World Precision Instruments), which when filled with working solution had resistances of 3–6 MΩ. Single-channel currents were amplified using an Axopatch 200B amplifier (Molecular Devices). The currents were filtered at 1 kHz and sampled at 10 kHz with a Digidata 1440A using pClamp 10 software. Negative pressures were applied using a high-speed pressure clamp (HSPC-1, ALA Sciences). A constant voltage of +30 mV was applied.

QUANTIFICATION AND STATISTICAL ANALYSIS

For the electrophysiology experiments, amplitude histogram with Gaussian fit enabled the calculation of single-channel conductance in Clampfit 10.7. In the main text and figures, n represents individual patches. Conductance and pressure threshold values represent the mean and standard deviation.

CryoEM data collection and processing were performed as described in the cryo electron microscopy section of the method details using CryoSPARC3.1.1,[95] RELION 3.1,[91] MotionCor2,[92] CTFFind,[93] and crYOLO.[94] Cryo-EM data collection and refinement statistics are summarized in Tables 1 and S1.